Supplementary Information

Improved performance of poly(vinyl pyrrolidone)/phosphonated poly (2, 6-dimethyl-1, 4-phenylene oxide)/graphitic carbon nitride nanocomposite membranes for high temperature proton exchange membrane fuel cells

Degree of phosphonation (DP) of PPO

The level of phosphonation of PPO was 42.36 % calculated from the data of ^{1}H-NMR. The degree of phosphonation (DP) was calculated from the average area B for six protons of $(CH_3CH_2O)_2$- at 1.2 ppm and C for four protons of $(CH_3CH_2O)_2$- at 4.02 ppm. The integral (A) of the signal at 6.5 ppm represents two protons of the aromatic proton ring in each repeating unit of the PPO. The areas for one proton of the phosphonate pendent would then equate to B/3 or C/2. The average area i.e. (1/2) {(B/6) + (C/4) } would then equal to a single phosphonate pendent. Since the area for a single proton at 6.5 ppm is A/2, the degree of phosphonation (DP) was then obtained by the following [1]:

$$DP = \frac{(1/2)\{(B/6)+(C/4)\}}{A/2}$$

The miscibility of PVP and pPPO

The miscibility of two polymer requires the components to form the homogeneous system, and its characteristic is that the glass-transition temperature (Tg) of the polymer blend is only one value, equivalent to fully compatible. If the polymer blending components both are amorphous, the blend membrane is transparent. Fig. S1 shown the photographs of the undoped and PA doped blend membrane and composite membrane. Fig. S2 (a) shown the DSC curves of PPO and derivatives. PPO and BPPO had a high glass-transition temperature (Tg) because of the rigidity of the polymer backbone. The Tg value of PPO with phosphonated side chain lowered due to the plasticizing effect [2], but the pPPO did not show any Tg in acid form. The absence of glass-transition for the polymer with phosphonic acid is commonly observed [2-5]. Fig. S2 (b) shown the DSC curves of PVP, pPPO and the blend membranes. The Tg value of PVP was about 180 ^{o}C. And the DSC curves of the PVP/pPPO blend membranes revealed the evanescence of glass transition with increasing the content of pPPO. So the results of DSC cannot show the miscibility of PVP and pPPO.

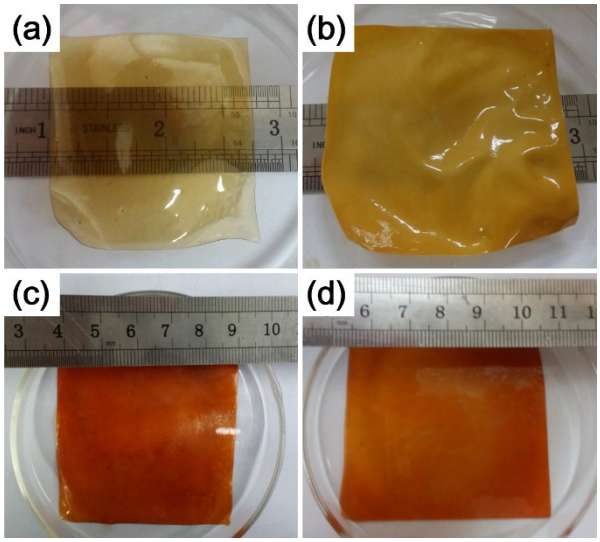

Fig. S1. Photographs of (a) 70%PVP/pPPO, (b) 70%PVP/pPPO/ g-C_3N_4 (5%), (c) PA doped 70%PVP/pPPO, (d) PA doped 70%PVP/pPPO/g-C_3N_4 (5%).

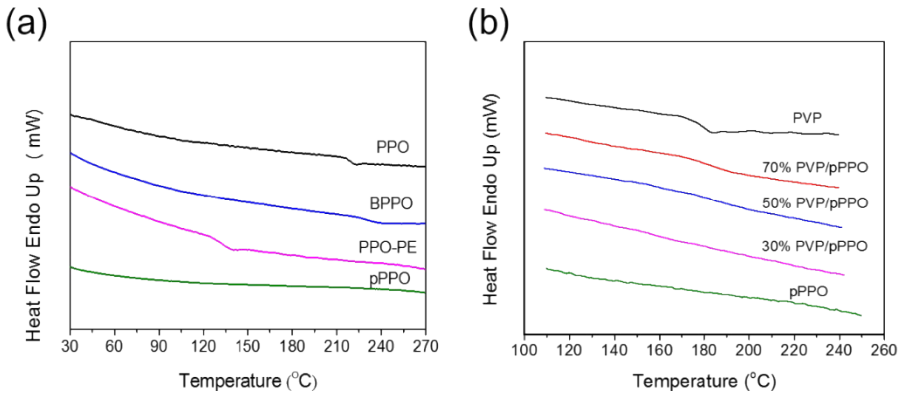

Fig. S2. DSC curves of (a) PPO and derivatives, (b) PVP, pPPO and the blend membranes.

If two kinds of polymer have very poor compatibility, the blend will present macro-phase separation, even appear stratified phenomenon, so being difficulty to the practical application. Fig.S3 shown the TEM micrographs of 70%PVP/pPPO and 70%PVP/pPPO containing 1 wt.% g-C_3N_4. The nanostructure without macro-phase separation of the blend indicated that PVP and pPPO had a relatively good compatibility. The g-C_3N_4 was also well dispersed in the blend polymer and individual nanosheet was observed at high magnification.

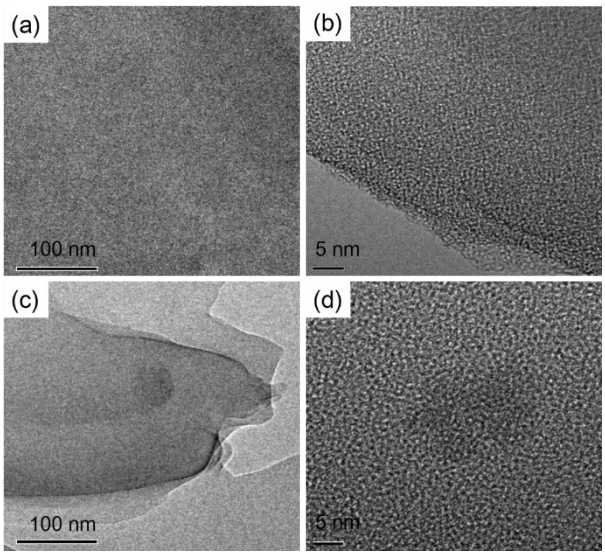

Fig. S3. TEM morphology of (a), (b) 70% PVP/pPPO and (c), (d) PVP/pPPO/g-C_3N_4 (1 wt.%).

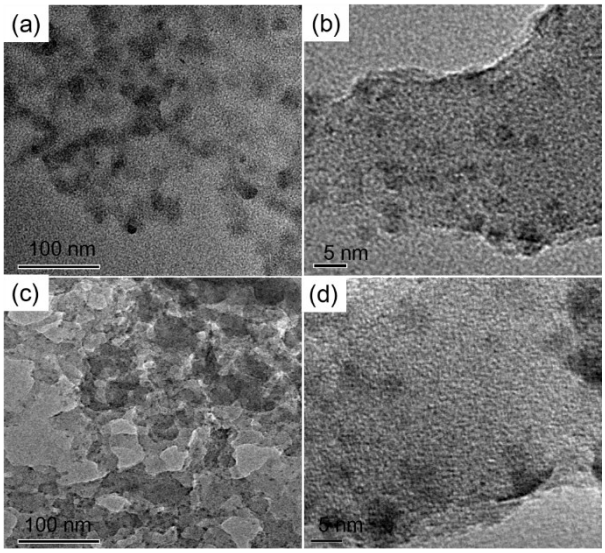

Fig. S4. TEM morphology of 70% PVP/pPPO/g-C_3N_4 (5%) (a), (b) and (10%) (c), (d).

Fig. S5 shown the XRD patterns of pPPO, PVP and PVP/pPPO blend membranes. The broad peaks for the pPPO and PVP indicated that they both were amorphous polymers. For the PVP/pPPO blend membranes, the PVP peaks covered the pPPO peaks due to the weak intensity. It stated that PVP and pPPO still maintained the amorphous structure.

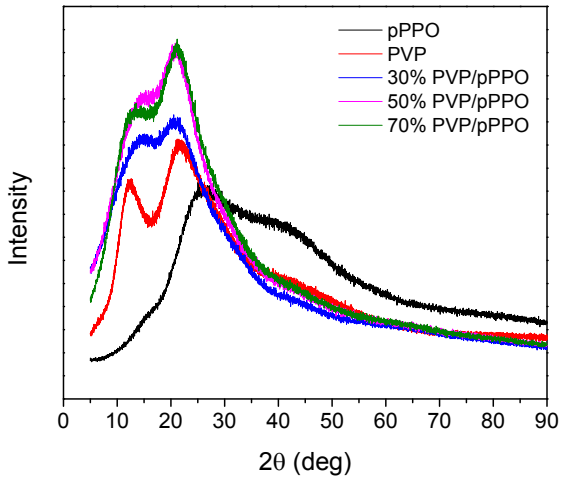

Fig. S5. XRD patterns of pPPO, PVP and PVP/pPPO blend membranes.

Acid doping level (ADL)

The PVP/pPPO blend membranes were immersed into 85 wt.% phosphoric acid (PA) at 80 °C for 24 h, then the PA doped membranes were taken out and wiped the PA on the surface with filter papers. The acid doping level (ADL) is defined as the moles of PA absorbed by per mole of PVP repeating unit. The ADL was calculated as below:

$$ADL = \frac{(W_{PA} - W_{dry}) / M_{H_3PO_4}}{W_{dry} \cdot \alpha / M_{PVPunit}}$$

where W_{PA} and W_{dry} are the membranes weights after and before PA doping treatment, α is the content of PVP in the blend membrane, $M_{H_3PO_4}$ is the molecular weight of H3PO4. $M_{PVPunit}$ is the molecular weight of PVP repeating unit.

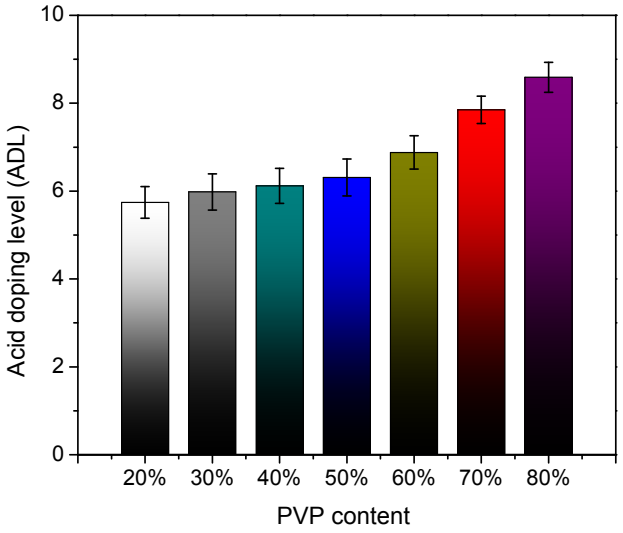

Fig. S6. Acid doping level of PVP/pPPO blend membranes at different PVP content.

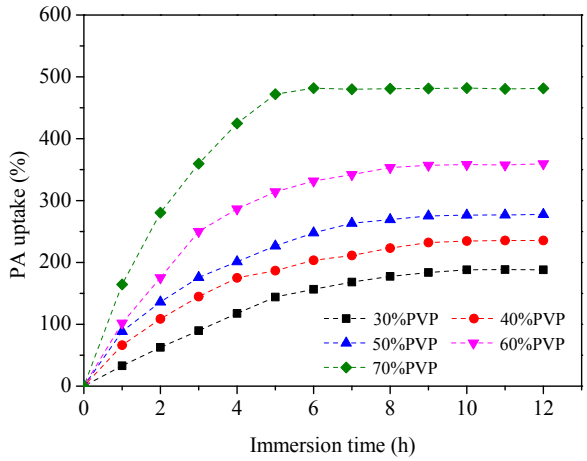

Fig. S7. PA uptake as a function of immersion time for PVP/pPPO blend membranes.

Table S1 Water uptake, PA uptake and acid doping level (ADL) of PVP/pPPO blend membranes.

	WU (%)		PA uptake (%)		ADL	
20%PVP	7.44	±0.8	101.36	±6.4	5.74	±0.36
30%PVP	19.78	±2.5	158.37	±10.8	5.98	±0.41
40% PVP	38.32	±2.0	216.30	±14.2	6.12	±0.40
50%PVP	59.04	±4.6	278.58	±18.7	6.31	±0.42
60% PVP	74.95	±6.4	364.43	±20.1	6.88	±0.38
70%PVP	130.29	±10.1	485.38	±19.5	7.85	±0.31
80%PVP	270.61	±18.2	606.72	±23.7	8.59	±0.34

Table S2 Dimensional change of PVP/pPPO blend membranes after PA doping

Swelling ratio	t (%)	L (%)	W (%)	V (%)
30%PVP	27.83 (±3.85)	31.74 (±4.21)	31.58 (±3.87)	125.54 (±10.23)
40%PVP	30.06 (±4.23)	33.05 (±3.84)	32.33 (±4.03)	143.74 (±13.74)
50%PVP	32.23 (±3.78)	35.80 (±5.31)	34.26 (±4.93)	177.17 (±12.67)
60%PVP	35.18 (±4.69)	38.97 (±4.72)	37.79 (±5.36)	190.91 (±16.38)
70%PVP	39.03 (±5.37)	42.43 (±5.53)	41.15 (±6.28)	237.39 (±19.59)

Characterization of g-C_3N_4

The morphology of g-C_3N_4 was investigated by FE-SEM and TEM. The sample of g-C_3N_4powder for SEM was placed on the conductive tape and the redundant particles were blew away with a rubber suction bulb. Then the sample was observed after having been coated a layer of gold. The sample for TEM was prepared by an ethanol solution of g-C_3N_4 dripping on an ordinary carbon film. Fig. 3 shows the SEM (a), TEM (b) images and XRD (c) pattern of g-C_3N_4. It could be seen that the g-C_3N_4 had the lamellar structure and small size. The g-C_3N_4 displayed aggregated morphology which contained small crystals with diameters of 60-400 nm. The selected area electron diffraction indicated that the g-C_3N_4 powder were crystalline particles with d ≈ 0.336 nm matched the (0 0 2) crystallographic plane of g-C_3N_4 (JCPDS 87-1526). The result of XRD pattern also confirmed the crystal structure of the g-C_3N_4 powder, which had two XRD peaks at 27.4°and 13.1° for (0 0 2) and (1 0 0) diffraction planes [6].

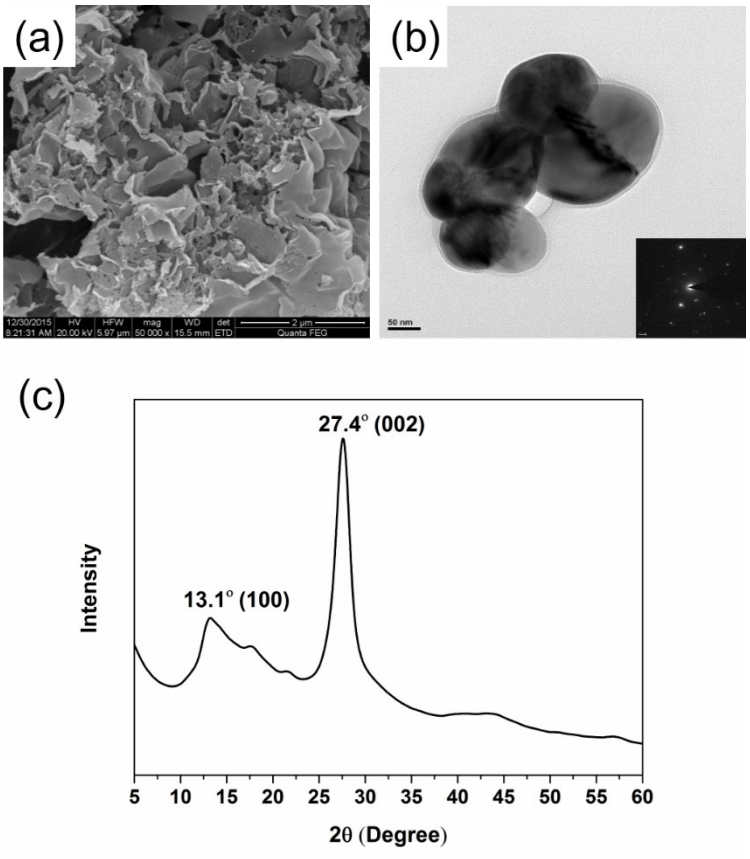

Fig. S8. The (a) SEM, (b) TEM images and (c) XRD pattern of g-C_3N_4.

Table S3. Mechanical properties of PA doped PVP-pPPO nanocomposite membranes.

Samples	Tensile strength (MPa)	Young's modulus (MPa)	Maximum elongation (%)
70%PVP-pPPO	1.49	8.76	18.43
1%g-C_3N_4	3.25	13.60	35.87
3%g-C_3N_4	4.35	16.97	48.14
5%g-C_3N_4	6.48	23.93	98.44
7%g-C_3N_4	5.78	27.87	62.45
10%g-C_3N_4	4.92	23.47	54.63

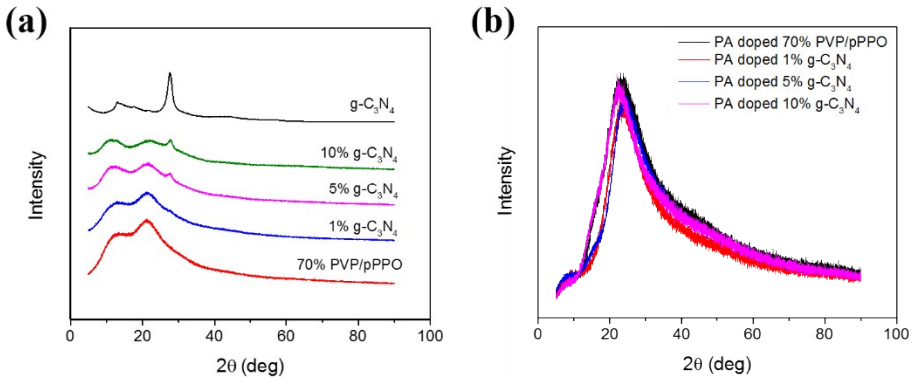

Fig. S9. XRD patterns of (a) g-C_3N_4, 70% PVP/pPPO blend and nanocomposite membranes. (b) PA doped 70% PVP/pPPO blend and nanocomposite membranes.

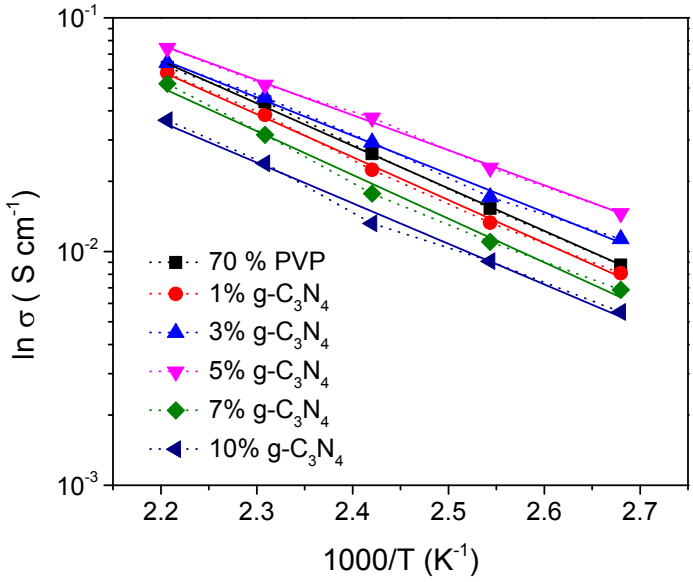

Fig. S10. Arrhenius-type temperature-dependent proton-conductivity behavior of the membranes.

Table S4. Comparison of proton conductivity with several PA doped membranes.

Membranes	PA uptake (wt.%)	σ (Scm^{-1})	Temperature (^oC)	RH%	Reference
70% PVP/pPPO	485 (7.85)	0.061	180	0	This work
PBI	200	0.042	180	5	7
PBI	(6.5)	0.033	120	20	8
PVP/PES	(9.1)	0.210	180	0	9
PES-PVP/PTFE	560	0.260	180	0	10
pPSU/PBI	210	0.038	170	25	11
PBI/PBI-BP	263	0.065	160	0	12
PEEK/PBI	277	0.081	200	0	13
SPEEK/PU	346	0.030	160	0	14
PVP/pPPO/g-C_3N_4 (5%)	471 (7.62)	0.074	180	0	This work
PBI/ (MWNT-poly(NaSS)) (0.3 wt%)	(14.7)	0.051	160	0	15
PBI /(MWNT-imidazole) (0.3 wt%)	(14.3)	0.043	160	0	15
PBI/clay (15%)	(8.9)	0.065	180	5	8
PBI/$SrCeO_3$ (8%)	190	0.105	180	0	16
PBI/ILGO (5%)	(3.5)	0.035	175	0	17
QPEEK/GO (7%)	193	0.075	200	0	18

* The value in the parenthesis refers to the PA doping level.

1. N. Y. A.-Thabit, S. A. Ali, S. M. J. Zaidi, New highly phosphonated polysulfone membranes for PEM fuel cells, J. Membr. Sci. 360 (2010) 26–33.
2. Julien Parvole and Patric Jannasch, Poly(arylene ether sulfone)s with phosphonic acid and bis(phosphonic acid) on short alkyl side chains for proton-exchange membranes, J. Mater. Chem., 2008, 18, 5547–5556.
3. K. Miyatake, A. S. Hay, New Poly(arylene ether)s with pendant phosphonic acid groups, Journal of Polymer Science: Part A: Polymer Chemistry, 39 (2001) 3770–3779.
4. V. Atanasov, J. Kerres, Highly phosphonated polypentafluorostyrene, Macromolecules 2011, 44, 6416–6423.
5. Z. Shao, A. Sannigrahi, P. Jannasch, Poly(tetrafluorostyrenephosphonic acid)–polysulfone block copolymers and membranes, Journal of Polymer Science: Part A: Polymer Chemistry, 2013, 51, 4657–4666.
6. X. Wang, X. Chen, A. Thomas, X. Fu, M. Antonietti, Metal-containing carbon nitride compounds: a new functional organic–metal hybrid material, Adv. Mater. 21 (2009) 1609–1612.
7. Y.-L. Ma, J. S. Wainright, M. H. Litt, R. F. Savinell, Conductivity of PBI membranes for high-temperature polymer electrolyte fuel cells, J. Electrochem. Soc. 151 (2004) 8–16.
8. D. Plackett, A. Siua, Q. Li, C. Pan, J. O. Jensen, S. F. Nielsenc, A. A. Permyakovab, N. J. Bjerrum, High-temperature proton exchange membranes based on polybenzimidazole and clay composites for fuel cells, J. Membr. Sci. 383 (2011) 78–87.

9. X. Xu, H. Wang, S. Lu, Z. Guo, S. Rao, R. Xiu, Y. Xiang, A novel phosphoric acid doped poly(ethersulphone)-poly(vinylpyrrolidone) blend membrane for high-temperature proton exchange membrane fuel cells, J. Power Sources 286 (2015) 458–463.
10. S. Lu, R. Xiu, X. Xu, D. Liang, H. Wang, Y. Xiang. Polytetrafluoroethylene (PTFE) reinforced poly(ethersulphone)–poly(vinyl pyrrolidone) composite membrane for high temperature proton exchange membrane fuel cells, J. Membr. Sci. 464 (2014) 1–7.
11. R. A. Potrekar, K. T. Clark, X. Zhu, and J. B. Kerr, Blend membranes of highly phosphonated polysulfone and polybenzimidazoles for high temperature proton exchange membrane fuel cells, ECS Transactions, 41 (2011) 2147-2159.
12. T.-H. Tang, P.-H. Su, Y.-C. Liu, T. L. Yu, Polybenzimidazole and benzyl-methyl-phosphoric acid grafted polybenzimidazole blend crosslinked membrane for proton exchange membrane fuel cells, Int. J. Hydrogen Energy 39 (2014) 11145-11156.
13. N. Zhang, C. Zhao, W. Ma, S. Wang, B.Wang, G. Zhang, X. Li, H. Na, Macromolecular covalently cross-linked quaternary ammonium poly(ether ether ketone) with polybenzimidazole for anhydrous high temperature proton exchange membranes. Polym. Chem. 5 (2014) 4939–4947.
14. Q. Che, N. Chen, J. Yu, S. Cheng, Sulfonated poly(ether ether) ketone/polyurethane composites doped with phosphoric acids for proton exchange membranes, Solid State Ionics 289 (2016) 199–206.
15. L. Jheng, C. Huang, S. L. Hsu, Sulfonated MWNT and imidazole functionalized MWNT/polybenzimidazole composite membranes for hightemperature proton exchange membrane fuel cells, Int. J. Hydrogen Energy 38 (2013) 1524-1534.
16. A. Shabanikia, M.Javanbakht, H. S. Amoli, K. Hooshyari, M. Enhessari, Polybenzimidazole/strontium cerate nanocomposites with enhanced proton conductivity for proton exchange membrane fuel cells operating at high temperature. Electrochimica Acta 154 (2015) 370–378.
17. C. Xu, X. Liu, J. Cheng, K. Scott, A polybenzimidazole/ionic-liquid-graphite-oxide composite membrane for high temperature polymer electrolyte membrane fuel cells, J. Power Sources 274 (2015) 922–927.
18. N. Zhang, B. Wang, Y. Zhang, F. Bu, Y. Cui, X. Li, C. Zhao, H. Na,. Mechanically reinforced phosphoric acid doped quaternized poly (ether ether ketone) membranes via cross-linking with functionalized grapheme oxide. Chem. Commun. 50 (2014) 15381–15384